

# Magnetohydrodynamics-induced internal crash near density limit in ohmic discharge on experimental advanced superconducting tokamak

L Q Xu<sup>1</sup>, Y M Duan<sup>1,3</sup>, W Shen<sup>1</sup>, Y Yuan<sup>1,2</sup>, Y Chao<sup>1,2</sup>, S T Mao<sup>1</sup>, S Y Lin<sup>1,3</sup>, K Y Chen<sup>1</sup> and L Q Hu<sup>1</sup>

<sup>1</sup>Institute of Plasma Physics, CAS Hefei, Anhui, 230031, People's Republic of China

<sup>2</sup>University of Science and Technology of China, Hefei, Anhui, 230026, People's Republic of China

E-mail: [ymduan@ipp.cas.cn](mailto:ymduan@ipp.cas.cn) and [linsy@ipp.ac.cn](mailto:linsy@ipp.ac.cn)

Received 2 July 2019, revised 10 December 2019

Accepted for publication 17 December 2019

Published 24 February 2020



## Abstract

The magnetohydrodynamics (MHD)-induced internal crash (IC) is one of the most fundamental dynamics of a tokamak discharge. Study of IC and the consequent formation of seed island (for neo-classical tearing modes) are still attractive in both experimental and numerical studies. In this work, a set of MHD-induced sawtooth like crashes (SLCs) have been observed in experimental advanced superconducting tokamak (EAST) ohmic discharge near density limit. With the tomography of high-resolution upgraded soft x-ray imaging system, it is observed that  $m/n = 2/1$  tearing mode converts to a  $m/n = 1/1$  instability, and it then triggers crash in the plasma core, here,  $m$  is the poloidal mode number and  $n$  is the toroidal mode number. Similar to sawtooth crash (SC), the crash of SLC here is due to  $m/n = 1/1$  mode nonlinear dynamic. An extended MHD simulation code M3D is used to understand of the dynamics of  $m/n = 1/1$  internal kink mode in SC in torus. A complex SC is reproduced from M3D nonlinear simulation under EAST realistic magnetic flux equilibrium and experimental resistivity. The rapid growth of unstable  $m/n = 1/1$  kink and interaction with its higher harmonics, are responsible for SC. The simulation results show an existence of annular chaos belt outside  $q = 1$  surface during SC. Furthermore, magnetic islands with higher poloidal mode number are found after SC. The formation of island after SC make plasma current profile flat in the core.

Keywords: soft x-ray tomography, tokamak diagnostics, MHD, 3D MHD nonlinear simulation

(Some figures may appear in colour only in the online journal)

## 1. Introduction

Internal crash (IC) is an internal magnetohydrodynamics (MHD) reconnection event that mixes plasma from the core and also the outer regions of tokamaks, cooling and flattening the central temperature and density profiles. Sawtooth crash (SC) is one of the most common type of IC when central safety factor  $q_0 < 1$ , which has character of an internal kink mode with dominant  $m/n = 1/1$ ,  $m$  is poloidal

mode number and  $n$  is toroidal mode number [1]. Sawtooth was first discovered in 1974, and many theoretical models have been developed to explain it, including Kadomtsev model [2] and Porcelli model [3], and so on. Experimental observations on HT-7 [4] and ASDEX-Upgrade [5] show the harmonics of  $1/1$  mode, e.g.  $2/2$  or  $3/3$  play an important role in SC. In ASDEX-Upgrade, it is also found that there is a chaos magnetic flux region near  $q = 1$  just before crash of sawtooth [5]. SC has been modeled in tokamak numerically with M3D [6, 7], NIMROD [8], XTOR-2F [9] and M3D + K [10].

<sup>3</sup> Authors to whom any correspondence should be addressed.

Another type of IC (termed as sawtooth like crash (SLC) in this paper) is similar to SC in consequence, but without inversion radius in radial. SLC was thought to be due to the interaction of two modes with identical toroidal numbers or double tearing modes. The toroidal MHD mode coupling due to the toroidal geometry of the tokamak and non-circular plasma cross-section was thought to be the dominant reason for SLC [11]. Discharge is usually not ended by repetitive SLC, this is exact same to SC. The cooling and flattening of temperature and density profiles caused by SLCs are not only in center but also extend to the plasma edge [12], this is different in the case of SC where the perturbations is limited by its mixing radius.

ICs, including both of  $m/n = 1/1$  internal kink triggered SC and multi-MHD (e.g.  $1/1$  and  $2/1$ ) induced SLCs, are deleterious to plasma confinement, limit the plasma  $\beta$ , and can generate run-away electron [13] and supply seed island for neoclassical tearing mode [14]. However, from the other side, ICs can be positive to the operation due to the avoidance of high-Z impurities accumulation [15, 16]. Furthermore, the core saturated  $m/n = 1/1$  kink mode themselves can cause significant current redistribution, which are favorable for so-called hybrid scenario via flux-pumping [17–20]. Understanding of internal kink is important for the operation of ITER where the  $q = 1$  radius could be as large as half of the minor radius.

In this paper, burst of SLCs near density limit in ohmic discharge have been investigated experimentally and SC is reproduced by M3D nonlinear simulation. Tomography of soft x-ray (SXR) show  $m/n = 2/1$  tearing mode converted to  $m/n = 1/1$  mode before crash. The crash mechanism of SLC is similar to SC, both of them due to the nonlinear dynamic of  $m/n = 1/1$  instability. SC driven by  $m/n = 1/1$  internal kink mode has been carried out by extend-MHD nonlinear simulation with M3D code under experimental advanced superconducting tokamak (EAST) realistic magnetic flux equilibrium and resistivity. The magnetic flux surface outside of  $q = 1$  becomes belt chaos during SC, which is due to the destabilization of harmonics. Islands with higher mode number are predicted after SC. The nonlinear simulation results qualitatively agree with EAST observations.

The rest of this paper is organized as follow: section 2 describes the diagnostics used in this work; a brief introduction of M3D is present in the section 3; section 4, gives the experimental observations of MHD-induced SLC near density limit in EAST; nonlinear simulation results about SC will be present in the section 5; in section 6, there will be a discussion and comparison between experimental observations and M3D simulation. Finally, a summary and future work plan will be present in section 7.

## 2. Upgrade of SXR imaging system on east and experimental description

EAST is a superconducting middle size tokamak with major radius  $R \sim 1.85$  m and minor radius  $a \sim 0.45$  m, can operate in many magnetic configurations with elongated factor

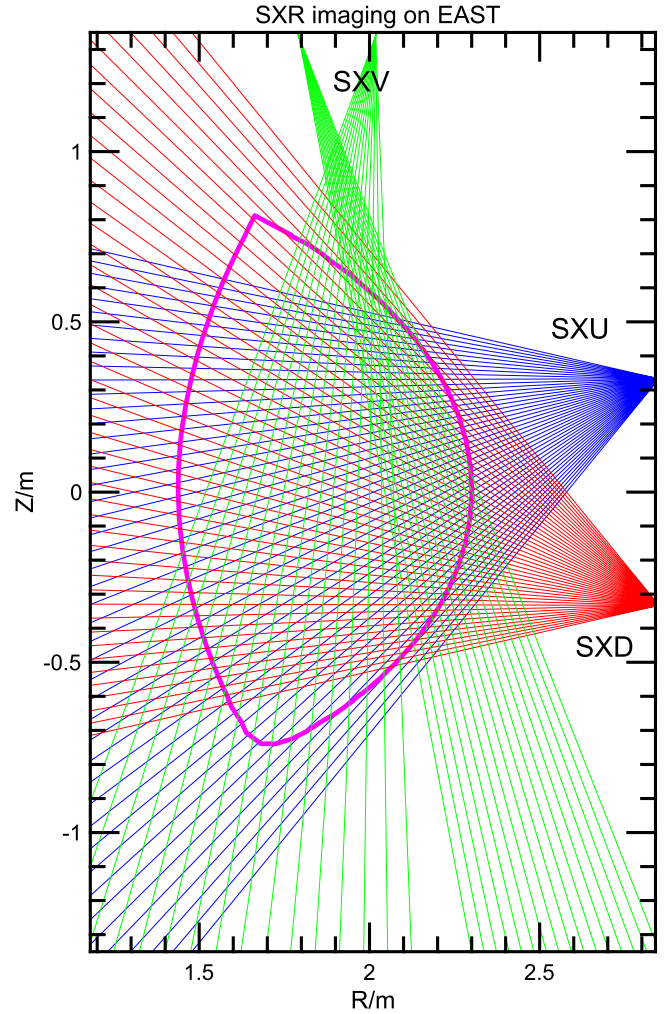


**Figure 1.** EAST SXR diagnostic consists with three full arrays with labels U, D and V. The sampling frequency of SXR is 100 kHz.

$\kappa \sim 1.7$  [21]. The SXR tomographic diagnostic used extensively in this paper is located in port P and the distribution of its integrating sightlines lie within a single poloidal plane as depicted in figure 1 [22]. The SXR diodes are filtered using  $12.5 \mu\text{m}$  Be foils. The SXR preamp voltage are digitized at 100 kHz which is enough to resolve the core MHD present since its frequency is less 10 kHz. The Fourier–Bessel method is used for SXR tomography and parameters  $l = 7$  and  $m = 2$  are selected. In 2019, the SXR in EAST has been upgraded, the new SXR diagnostic has three full arrays to cover complete plasma poloidal section, which makes it possible to reconstruct  $m = 2$  mode and to investigate the  $2/1$  induced SLC in detail.

Electron cyclotron heterodyne radiometer diagnostic is used for identification of  $m = 2$  island and determination of location of  $q = 2$  surface. Electron cyclotron heterodyne radiometer provides temperature of electron based on measurements using optically thick, second harmonic (X-mode) electron cyclotron emissions (ECEs) in 32 radial locations, with a 1 MHz sampling rate in the tokamak mid-plane [23, 24]. Local flattened O-point profile is used to indicate the formation of a large island and the inversion radius between

two radial channels with a  $\pi$  jump in the phase is recognized as the location of rational surface [25].

The experiment data present in this work are taken from EAST two ohmic discharges #48387 and #83477 in 2014 and 2019, respectively. Those two ohmic shots have same MHD-induced SLCs near density limit operation. The MHD dynamics of radiation driven  $m = 2$  island and the consequent SLCs has been reported in detail in our previous work in 2014 [12], which mainly using ECE diagnostic. In 2019, the dynamics of radiation driven  $m = 2$  island near density limit in ohmic discharge has been re-analyzed with the upgraded SXR diagnostic.

Gates *et al* proposed a mechanism that explains the density limit using a thermo-resistive tearing mode formalism [26–28]. The power balance of magnetic island is dominated by radiative cooling and ohmic heating, because it is thermally isolated. The internal temperature profile of the island is determined by the local power balance. Radiative cooling increase as the increase of plasma density, and then ohmic heating typically decreases in the case of fixed toroidal electric field potential. The temperature drop creates a negative current perturbation inside the island if radiation losses dominate. The current perturbation, coupled with the asymmetry of the island, can cause substantial growth of the island and lead to disruption [28]. However, as shown in [12], if the growth of radiation-driven island has interrupted, e.g. the mode converted to other inner mode, SLCs will happen instead of major disruption.

Two discharges with same SLC dynamics in ohmic shot near density limit selected for analysis in this work. The repetitive burst of mode dynamics and the consequent SLCs are shown in MC signals and core ECE signals respectively in figure 2. One should be note that the MHD shown in MC are  $m/n = 2/1$  tearing mode, which characterized with the formation of  $m = 2$  island (see [12] and [appendix](#)).

### 3. Extended MHD simulation code M3D

M3D solves the following full MHD resistive equations in the torus,

$$\rho \partial V / \partial t + \rho V \cdot \nabla V = -\nabla p + J \times B + \mu \nabla^2 V \quad (1)$$

$$\partial B / \partial t = -\nabla \times E, J = \nabla \times B, \nabla \cdot B = 0 \quad (2)$$

$$E = (-V \times B + \eta J) \quad (3)$$

$$\partial \rho / \partial t + \nabla \cdot (\rho V) = 0 \quad (4)$$

$$\partial p / \partial t + V \cdot \nabla p = -\gamma p \nabla \cdot V + \rho \nabla \cdot \tilde{\kappa} \nabla (p / \rho). \quad (5)$$

Equation (1) is momentum equation, equation (2) is Maxwell, equation (3) is Ohm law, equation (4) is continuity and equation (5) is for energy. Where,  $\rho$  is mass density,  $V$  is fluid velocity,  $p$  is pressure,  $J$  is current density,  $B$  is magnetic field,  $E$  is electric field,  $\mu$  is viscosity,  $\eta$  is resistivity,  $\gamma$  is the ratio of specific heats = 5/3 for an adiabatic system, and  $\tilde{\kappa}$  is the thermal conductivity tensor. The equilibrium used in this paper is calculated from kinetic-EFIT, which includes the experimental electron density and temperature [29].

We consider an ohmic discharge with shot number 48387 near density limit in EAST tokamak for M3D nonlinear simulation. In this discharge,  $m = 2$  island around  $q = 2$  surface has been found due to the edge cooling effect.  $m/n = 2/1$  tearing mode converts to  $m/n = 1/1$  mode and the growth of 1/1 mode leads to SLC [12]. There is no inversion radius in radial for SLC, which is thought as a typical character for SC [30].

The main parameters and profiles of shot #48387 are follows: major radius  $R_0 = 1.85$  m, minor radius  $a = 0.45$  m, inverse aspect ratio  $\epsilon = \frac{a}{R_0} = 0.24$ , elongation  $\kappa = 1.34$ , triangularity  $\delta = 0.37$ , toroidal magnetic field  $B_0 = 2.25$  T, electron density in the core  $n_{e0} = 6.37 \times 10^{19} \text{ m}^{-3}$ , electron temperature in the core  $T_{e0} = 0.55$  keV. The central plasma beta  $\beta_0 = 0.56\%$ , the calculated Alfvén speed in the core  $v_{A0} = 4.35 \times 10^6 \text{ m s}^{-1}$ , Alfvén time  $\tau_{A0} = 4.25 \times 10^{-7} \text{ s}$ , the resistive time  $\tau_R = 1.72 \text{ s}$  and the correspondingly Lundquist number  $S = \frac{\tau_R}{\tau_A} = 4.05 \times 10^6$ . The current factor inductance  $li = 1.65$  and effective charge number in the core  $Z_{\text{eff}0} = 2.9$ . With the above experiment data, the key parameters are set as followings for M3D nonlinear simulations:

$$\eta = \frac{1}{S} = 2 \times 10^{-7}, = 1 \times 10^{-5} (\epsilon a v_{A0}), \chi_{\perp} = 1 \times 10^{-5}$$

( $B_0^2 R_0 / v_{A0}$ ) and  $q_0 = 0.84$ . The edge  $q$  factor is  $q_{95} = 5.6$  for this typical shot, the  $q$  profile, current profile and pressure profile are shown in figure 3. The artificial sound implementation of parallel heat conduction was switched on in M3D. The growth rates of high  $n$  are reduced by the addition of a realistic level of parallel heat conduction and can be stabilized by the additional imposition of a large perpendicular thermal conductivity coefficient. Both parallel and perpendicular heat conduction were employed, stabilizing the higher- $n$  modes.

### 4. Experimental observations

Crashes induced by interaction of MHD modes have been studied widely both in the tokamak experiment and theory [31–36]. In our previous study, the measurements of ECE have revealed that 2/1 island can be driven by plasma radiation near density limit in ohmic discharge and SLC can be triggered in the case of  $m/n = 2/1$  tearing mode transition to  $m/n = 1/1$  instability [12]. In this work, a new upgraded SXR diagnostic has detected those SLC also. As describe in section 2, the SXR tomography diagnostic has been upgraded in 2019. The Fourier–Bessel technology with parameters  $l = 7$  and  $m = 2$  was used for SXR reconstruction. Figure 4 shows a set of SLCs at the plasma current ramp-down phase, where the plasma density is approaching to Greenwald limit. The parameters of discharge No. 83477 are, plasma current in the top-flat  $I_p = 400$  kA and the electron density in the core  $n_{e0}/n_G = 0.5$ .  $n_G = I_p / \pi a^2$ ,  $I_p$  is the total plasma current, and  $a$  is the plasma geometric minor radius. In (f) of figure 4, three core SXR channels indicate a clear crash. The perturbations of MHD measured by SXR raw line-integrated data show clear  $m = 2$  structure in time 1 and  $m = 1$  structure in time 4 at (g) of figure 4. The frequency of  $m = 2$  mode

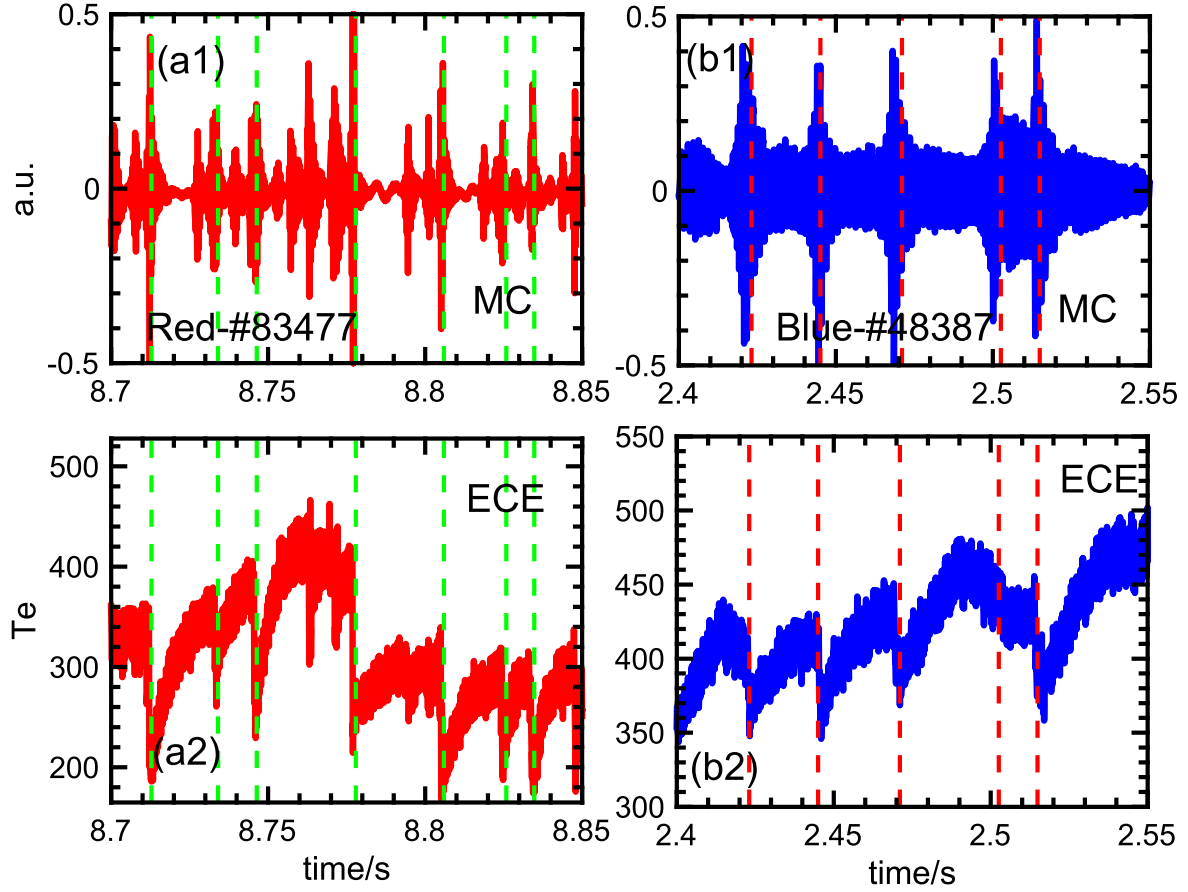


**Figure 2.** MHD-induced SLCs in two ohmic shots (#83477 & #48387) near density limit. (a1)—edge Mirnov coils (MC) of #83477; (b1) MC of #48387; (a2) ECE of #83477 and (b2) ECE of #48387. Both MHD in 83477 and 48387 detected in MC are  $m/n = 2/1$  tearing mode.

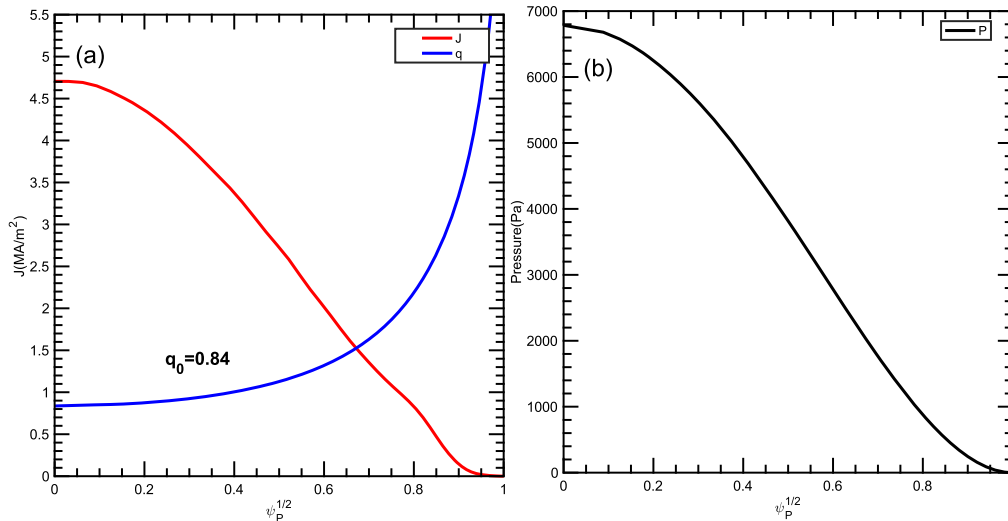


**Figure 3.** Equilibrium profiles of current,  $q$  and pressure in EAST shot #48387. The safety factor is below unity in the axis.

measured by edge MC is about 2 kHz (figure 4(e)). Zoomed raw data of SXR show a very clear  $m = 2$  to  $m = 1$  process (figure 4(j)).

Tomographic reconstruction from SXR brightness profile provide clear 2D structures of SLC. In this work, singular value decomposition (SVD) is employed to extract the

perturbation of SXR brightness profiles. The evolution of mode structures during crash are shown in figures 4(h) and (i). At time 1, the reconstruction of SXR perturbation show  $m = 2$  structure near  $q = 2$  surface. Here,  $q = 2$  surface is determined from ECE measurement. The hot core of SXR profile is circular in the center, which is totally different to



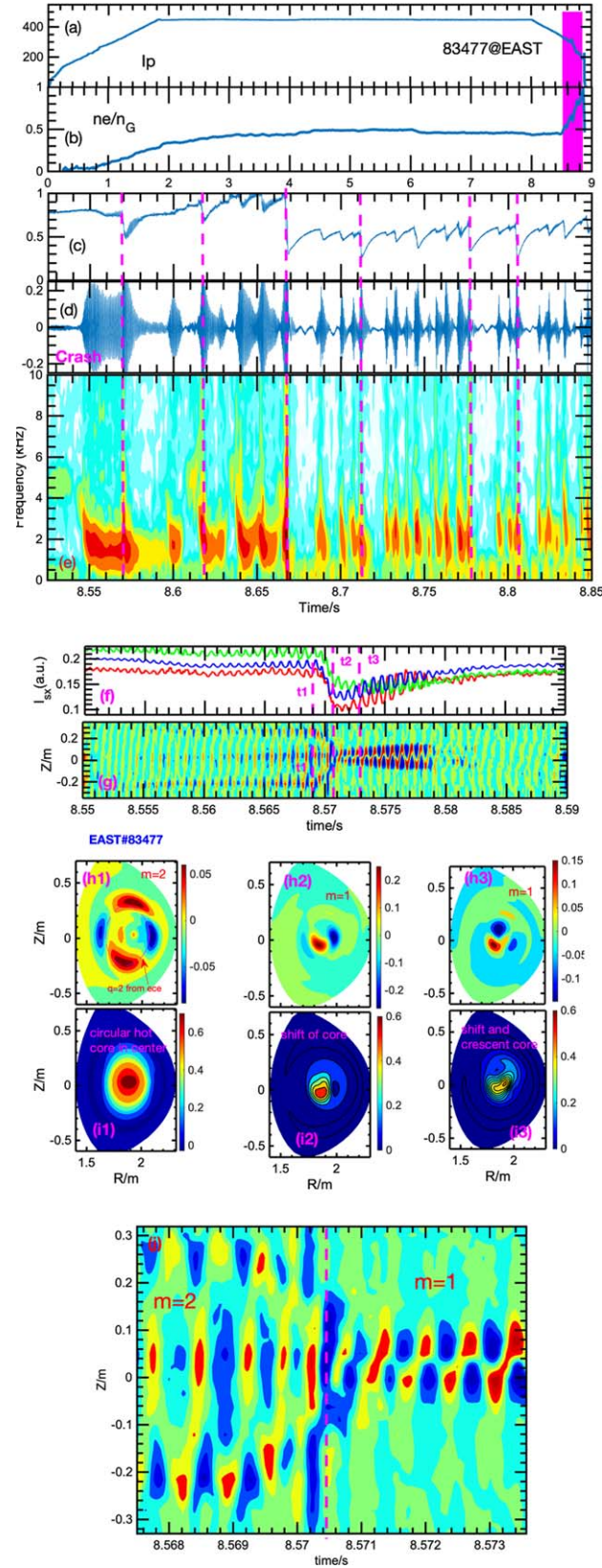


**Figure 4.** SXR tomographic study of  $m/n = 2/1$  mode induced SLC near density limit of discharge No. 83477 on EAST. (a)—plasma current  $I_p$ ; (b)—line-integrated electron density  $n_{e0}/n_G$ ; (c)—core SXR; (d)—edge Mirnov coil (MC) of  $m/n = 2/1$ ; (e)—frequency spectrum of MC in (d); (f)—(i)—tomography of a typical SLC, (f)—three SXR channels of SLC; (g)—contour plot of the evolution of SXR perturbation profiles for SLC,  $m = 2$  in time 1 and  $m = 1$  in time 4; (h)—contour plot of reconstructed perturbation of the local emission intensities from the perturbation signals extracted by the SVD method; (i)—contour plot of the reconstructed local emission intensities profile from total signals. The three frames in (h) and (i) correspond to those in the frame (f) and frame (g); (j)—zoomed plot of (g).

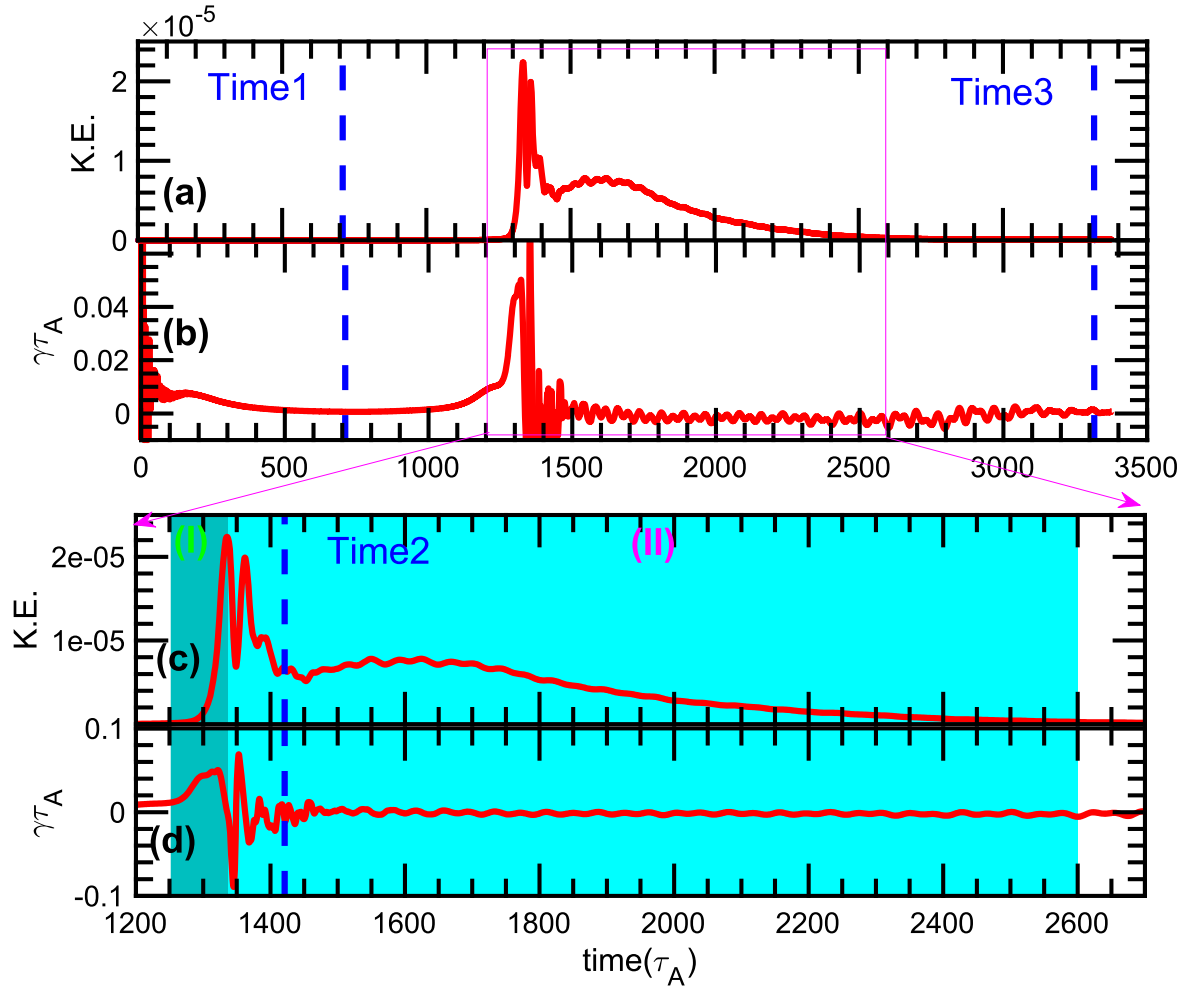


**Figure 5.** Complex SC predicted by M3D nonlinear simulations with  $n$  up to 8. (a)—total kinetic energy (ke); (b)—growth rate (g); (c) and (d) the zoomed of internal crash of (a) and (b), respectively. The color highlighted phase (I) is the growing phase, similar to precursor growing phase before sawtooth crash; phase (II) is the complex crash. The complex manifests as gradually decay with aperiodicity oscillations.

1/1 kink, e.g. sawtooth precursor. In the second phase, double hot spots associated to  $m = 2$  mode coalesce into one big spot in the high field side (figure 4(h2)) and the hot core is tiny shift away of plasma center (figure 4(i2)). At this time, a very strong 1/1 mode appears in the tomographic pattern, and the hot core largely shift away of plasma core. In time 3, the hot core becomes crescent, which indicates a formation of  $m = 1$  island. After crash, the  $m = 2$  mode is very weak, appearance as small oscillations in SXR signals at  $t = 8.585$  s (figure 4(f)). Those observations are consistent with ECE measurements in our previous work [12].

## 5. M3D Nonlinear simulation results

EAST observations from SXR tomography (figure 4) and ECE [12] show that SLC is corresponding to the dynamics of  $m/n = 1/1$  kink instability. In this section, we apply M3D code to consider the nonlinear evolution of the internal kink mode with  $n = 1$ . Up to 24 toroidal planes corresponding to  $n$  up to 8

is used in nonlinear simulation. The plasma is modeled by single fluid MHD equations, which include the dissipative processes associated with viscosity  $\mu$  and electrical resistivity  $\eta$ . EAST realistic magnetic equilibrium flux from k-EFIT for shot #48387 is used in M3D simulation. The other main input parameters are  $\mu = 1 \times 10^{-5}$ ,  $\eta = 2 \times 10^{-7}$ ,  $\nu = 1 \times 10^{-5}(\epsilon a v_{A0})$ ,  $\chi_{\perp} = 1 \times 10^{-5}(B_0^2 R_0 / v_{A0})$  and  $q_0 = 0.84$ . Note that the resistivity  $\eta$  used here is the experimental value.

A complex SC is modeled by nonlinear simulation. SC is due to the nonlinear dynamics of the unstable  $m/n = 1/1$  internal kink mode. The evolution of simulated total kinetic energy and the growth rate are shown in figures 5(a), (b). Figures 5(c) and (d) present the detail of the complex crash. Three times marked with Time 1, Time 2 and Time 3 are long before crash, during crash and long after crash, respectively, will be selected for investigated in detail in the rest of this work.

In figure 6, the nonlinear simulation results show unstable internal kink mode with growth rate  $\gamma_{\tau_A} \sim 0.01$  and with  $U_{\max} \sim 1.1 \times 10^{-4} \left( \int^2 v_A \right)$  before mode growing. After  $1200 \tau_A$ , the unstable 1/1 internal kink mode start to grow.

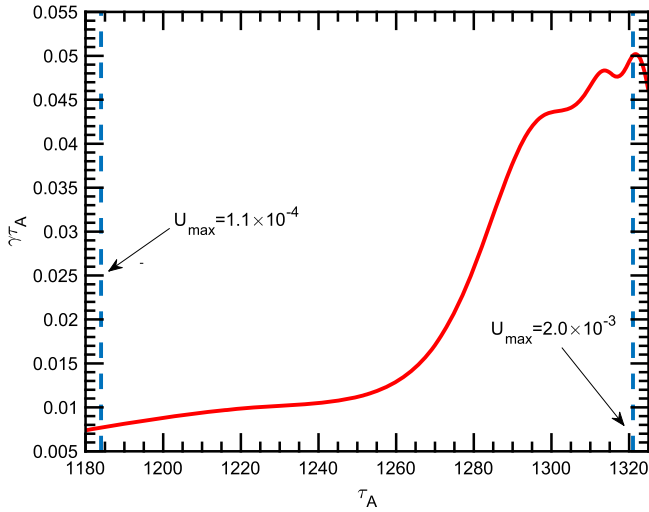


**Figure 6.** Rapid growth of 1/1 kink mode before crash. The growth rate increased from  $\gamma\tau_A \sim 0.01$  to  $\gamma\tau_A \sim 0.05$  within  $t = 100\tau_A$ , and the corresponding kink mode grows from  $U_{\max} = 1.1 \times 10^{-4}$  to  $U_{\max} = 2.0 \times 10^{-3}$ ,  $U$  is velocity stream function.

The unstable 1/1 internal kink mode grows nonlinearly with exponent index in the following  $100\tau_A$ . The growth rate increased from  $\gamma\tau_A \sim 0.01$  to  $\gamma\tau_A \sim 0.05$ , and the corresponding kink mode grows from  $U_{\max} = 1.1 \times 10^{-4}(\epsilon^2\vartheta_A)$  to  $U_{\max} = 2.0 \times 10^{-3}(\epsilon^2\vartheta_A)$  before crash. Where,  $U$  is the velocity stream function. The growing phase  $t = 100\tau_A \sim 0.05$  ms ((I) in figures 5(c), (d)) is comparable with the time of sawtooth precursor. Note that the time of sawtooth precursor is much slower than time of sawtooth quiescent ramp-up. The growth of sawtooth precursor is very fast and in some particular case that time is too short to detect for experiment [37–39]. The crash of complex phase is about  $t = 1500\tau_A \sim 0.75$  ms ((II) in figures 5(c), (d)), which agrees with crash time of SLC on EAST (See figure 4(c)).

We now compare the mode characters on the three different times as marked in figure 5. Figures 7(a) and (b) show the electron perturbations  $\delta T_e$  and magnetic flux perturbations  $\delta\psi$  in three times. The magnitudes of the perturbed poloidal harmonics  $m$  for the 1/1 kink mode are determined relative to the equilibrium magnetic flux surface coordinate system  $(\rho, \theta)$  and plotted against normalized  $\rho$ . Shown in the figures 7(c) and (d) are harmonics  $m$  of  $\delta T_e$  and  $\delta\psi$ , respectively. Poincare plots of magnetic surfaces at the  $\varnothing = 0$  toroidal plane at the three corresponding times are present in figure 7(e).

Time 1 shows the eigenfunctions of the  $m/n = 1/1$  internal kink mode. It is notable that 2/1 component of  $n = 1$  kink mode of magnetic flux is comparable to 1/1 component in  $q = 1$  surface (figures 7(b1) and (d1)).  $\tilde{\psi}_{21}/\tilde{\psi}_{11} = 2.1 \times 10^{-6}/5.5 \times 10^{-6} = 38\%$  at  $q = 1$  surface for 1/1 kink mode in torus. There is no shift in core in Poincare plot of magnetic surface for 1/1 eigenfunction (figure 7(e1)). The eigenfunction of temperature perturbation  $\delta T_e$  for 1/1 kink is dominant with  $m = 1$  component and high harmonics are tiny (figures 7(a1) and (c1)).

During crash (Time 2), 1/1 mode expands out and harmonics are developed, the magnitude of  $\delta T_e = 1.2 \times 10^{-3}$ .

As shown in figure 7(a2), there is an annular region formation out of  $q = 1$  surface due to the destabilization of harmonics, which is similar to experimental observation of off-axis sawtooth crash SC on TFTR [40]. Figures 7(c2) and (d2) indicates the expansion of  $m = 1$  component and grow of harmonics, e.g.  $m = 2$ . The magnetic is core-shifted due to the large  $n = 1$  kink instability and an annular stochastic region near  $q = 1$  surface is found, as Poincare plot in figure 7(e2).

After IC (Time 3), harmonic modes extend to the  $q = 2$  surface (figures 7(a3) and (c3)) and a strong  $m = 4$  is found (figures 7(b3) and (d3)). Decomposition of poloidal structure show double  $m = 1$  mode, a small one in inner and a very big one in outer of electron temperature perturbations (figure 7(c3)). The harmonics of magnetic flux perturbations are different to  $\delta T_e$ , there is also double  $m = 1$  mode, but the larger one is the inner one. In addition, strong  $m = 2$  and  $m = 4$  component of  $\delta\psi$  are predicted.

It is very important to point out, the toroidal number here is not  $n = 1$  only (for time 2 and time 3), but couples with its harmonics, e.g.  $n = 2$  and  $n = 4$ , as shown in figure 8. The Poincare plot of magnetic surface in figure 7(e3) show  $m = 4$  islands formation after crash. The eigenfunction of the 1/1 kink mode has not 1/1 structure but 2/1 for  $\delta\psi$ , as shown in figures 7(d1) and 8(b1). The initial perturbations of 1/1 kink mode should be same with linear simulation, which also used for mode eigenfunction structure and mode growth rate (or frequency) study.

As mentioned above, magnetic island with high- $m$  is seen after crash, this is a very interesting result, which agree with many experimental observations [11, 14, 41]. To verify the existence of magnetic island, we project the parameters of plasma current  $J$  and plasma pressure  $P$  to equatorial plane ( $Z = 0$ ). The results are shown in figure 9. The pressure and current profile become flat after crash. The formation of magnetic islands with high mode numbers lead to current profile flatten after crash.

As mentioned in figures 5(c) and (d), the nonlinear M3D simulation predicted crash has more than one crash, which is similar in shape to the compound SC observed in many tokamaks [42–45], however, it is not compound sawtooth here, compound sawtooth consists with more than two crashes in experiment, and the simulation here is a complex crash process only. We now investigate the complex crash process in detail. Two timepoints, one is after first crash-oscillation and the other is after second crash-oscillation are selected for analyses. The results are shown in figure 10. After the first crash-oscillation,  $m = 2$  component is the biggest, the magnetic flux in the core has been stretched symmetry. The core is not shifted to high field side or lower field side (figures 10(b1), (c1)). The higher  $m = 3$  and  $m = 4$  components are smaller than  $m = 1$  (figure 10(d1)). However, after second crash-oscillation, the  $m = 4$  component becomes stronger than  $m = 2$ , and  $m = 1$  is comeback to the largest one (figures 10(b2), (c2)). Poincare plots of magnetic surface show  $m = 4$  islands formation and the core are small shift to the high filed side (figure 10(d2)). The annular stochastic regions are found in both of crash-oscillations.

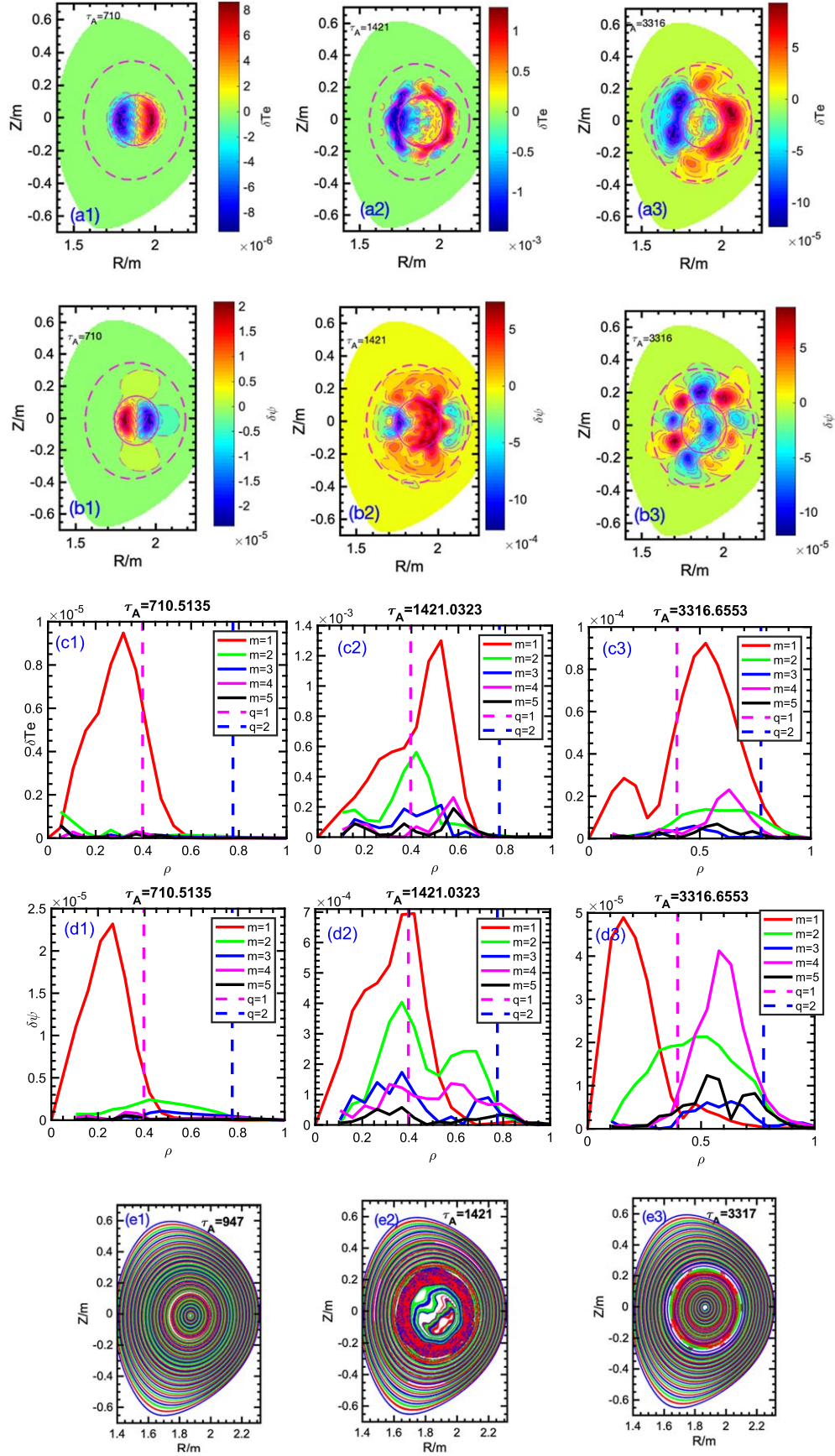


**Figure 7.** Evolution of the electron perturbations  $\delta T_e$ , magnetic flux perturbations  $\delta\psi$  and Poincare magnetic surfaces for 1/1 induced crash. (a1)–(a3),  $\delta T_e$ ; (b1)–(b3),  $\delta\psi$ ; (c1)–(c3), flux-surface-coordinate poloidal harmonics for (a1)–(a3); (d1)–(d3), flux-surface-coordinate poloidal harmonics for (b1)–(b3); (e1)–(e3), Poincare plots of magnetic surface in three times.



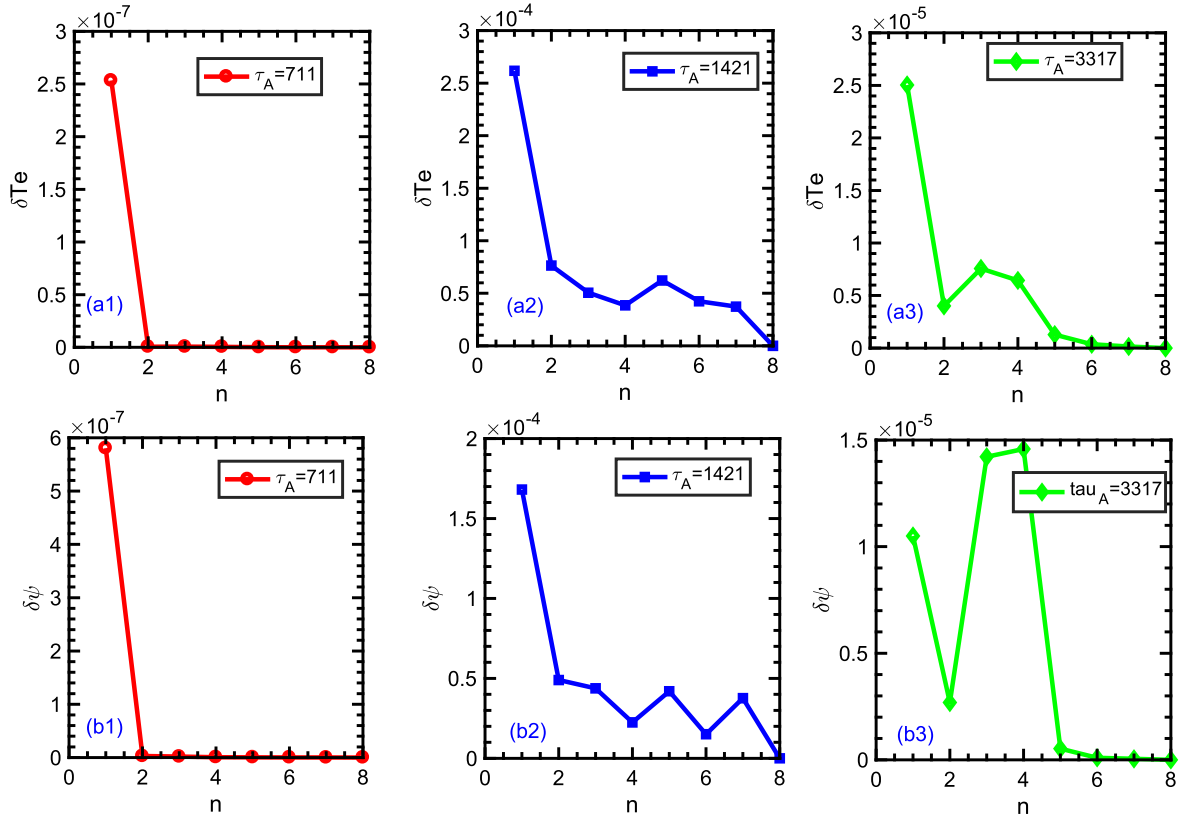


**Figure 8.** The profiles of toroidal mode number  $n$  in three times for  $\delta T_e$  and  $\delta\psi$ . (a1)–(a3)— $\delta T_e$ ; (b1)–(b3)— $\delta\psi$ .

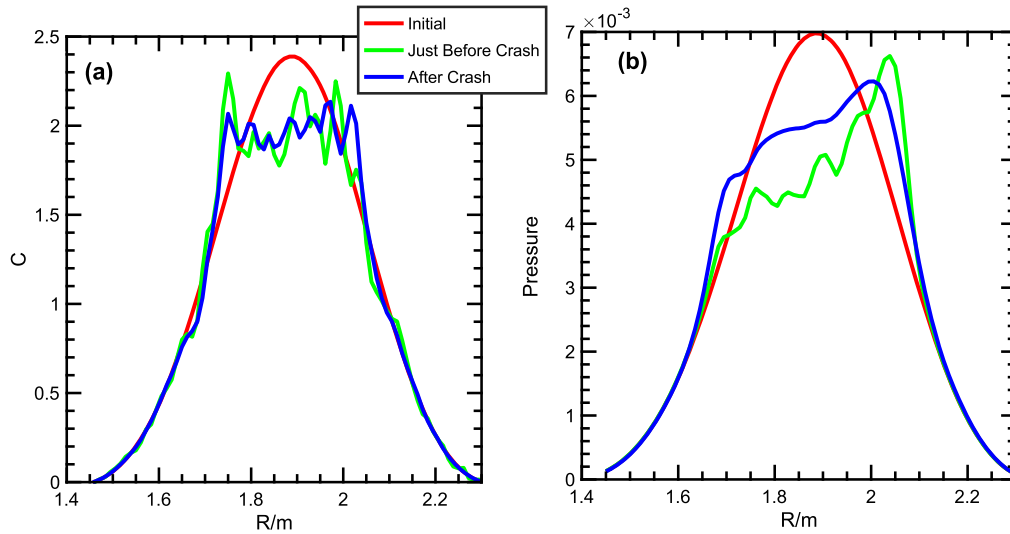


**Figure 9.** Current  $J$  and pressure  $P$  profiles evolution associated with crash. (a) Current  $J$ ; (b) pressure  $P$ . The current profile is flat in the core after crash cure.

The nonlinear simulation about  $m/n = 2/1$  tearing mode and the associated island dynamics with experimental values (e.g.  $\eta$ ,  $\mu$ ,  $\psi$ ) have been carried out. Because of a much longer computation time is required for the slower growth of tearing mode, we do not find crash due to the growing of  $m = 2$  island. The eigenfunction of flux perturbations, velocity stream function and pressure perturbations show  $m/n = 2/1$  structure in M3D nonlinear simulation for EAST, as shown in figure 11. It is found the growth rate of  $2/1$  island

is  $\gamma\tau_A = 1.35 \times 10^{-4}$ , which is about two order slower than  $1/1$  internal kink mode  $\gamma\tau_A = 0.01$  (figure 6).

## 6. Discussion and comparison between simulation and experiment

The edge cooling due to strong radiation loss can drive  $m/n = 2/1$  tearing mode and lead to series of SLCs in the

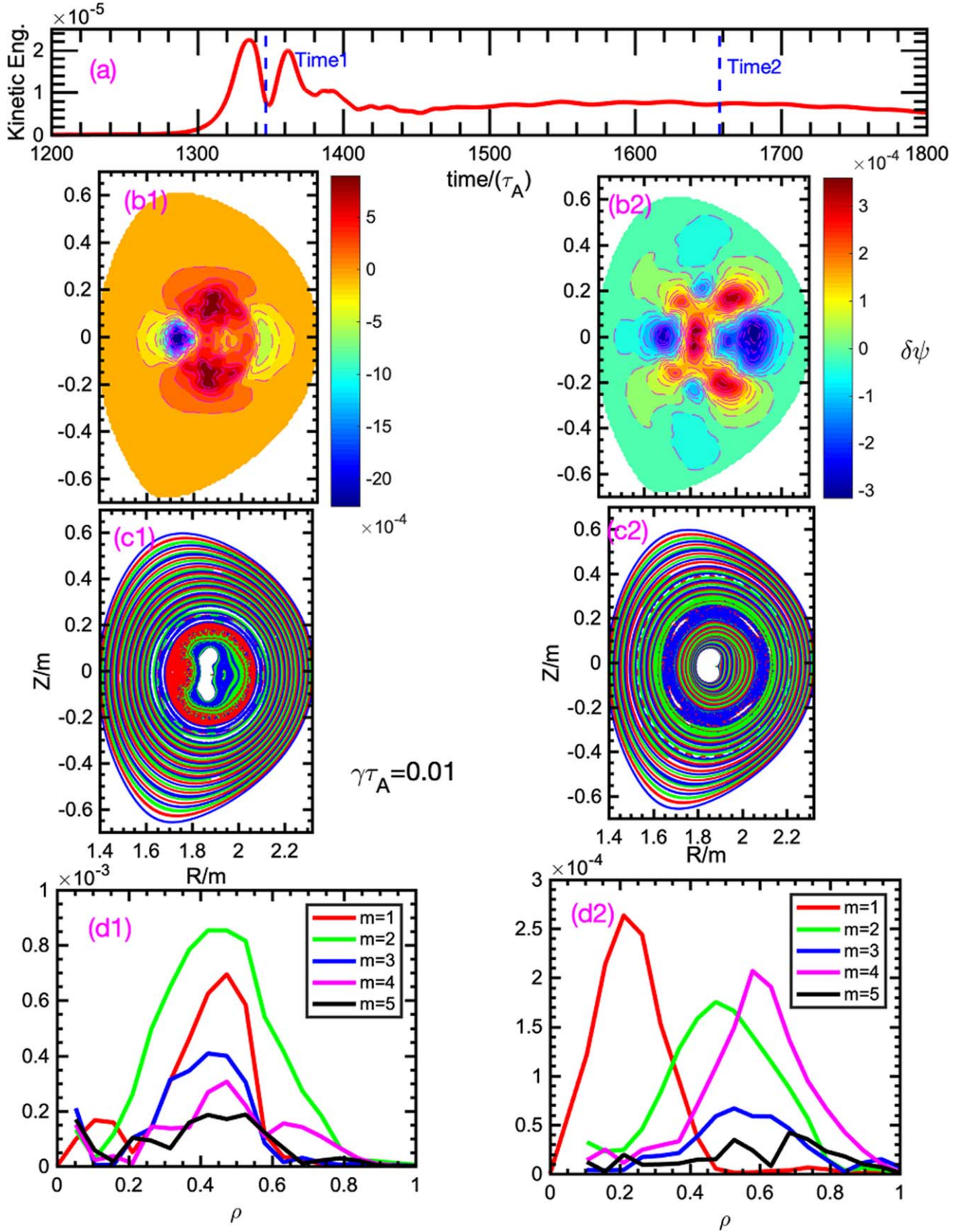


**Figure 10.** Compare of parameters in two crash-oscillations. (a)—Time evolution of total kinetic energy ( $n = 1-8$ ); (b)—contour plots of  $\delta\psi$ ; for time1 and time2 (c)—Poincaré plots of magnetic surface at two times  $\delta\psi$ ; (d)—poloidal harmonics of  $\delta\psi$  for two times (b). The two frames in (b)–(d) correspond to timepoints in the frame (a).

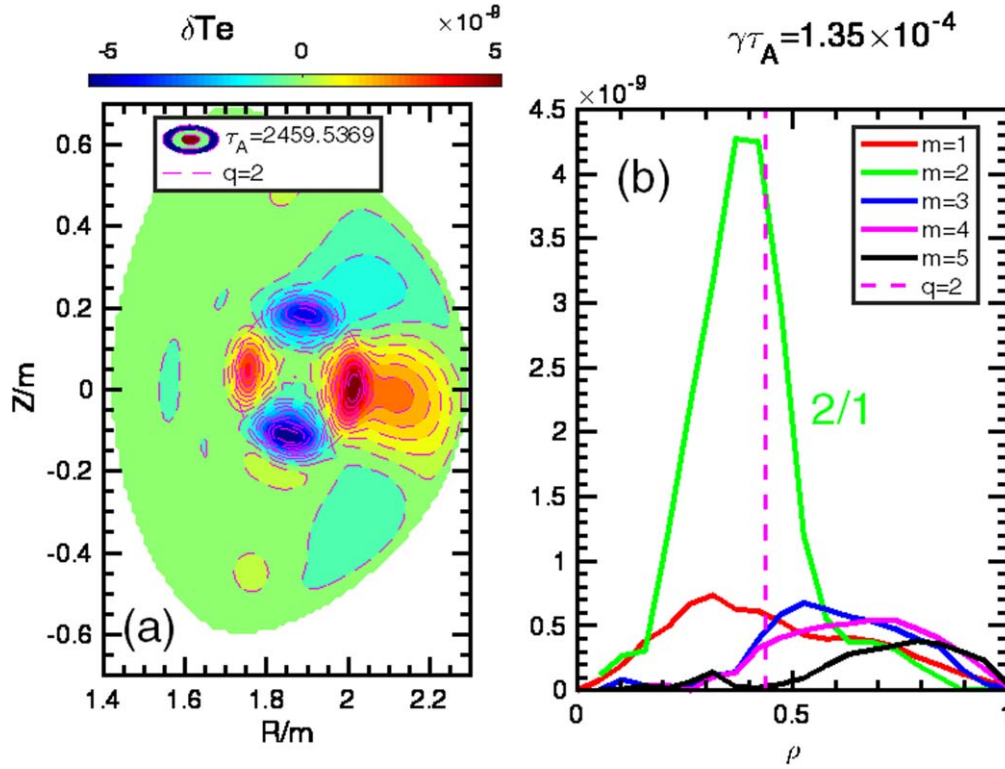


**Figure 11.** Examples of 2/1 mode nonlinear simulation with M3D. (a) Contour plots of  $\delta T_e$  (b)—poloidal harmonics of  $T_e$ . Growth of  $m = 2$  resistive island ( $\gamma_{TA} = 1.35 \times 10^{-4}$ ) is about two order slower than IC ( $\gamma_{TA} = 0.01$  (figure 6)).

core or ultimately trigger major disruption near density limit in EAST ohmic discharge. With the tomography of upgraded SXR diagnostic, a set of SLCs have been found in EAST experiment. SLC is due to the nonlinear growth of 2/1 tearing mode induced  $m/n = 1/1$  mode, which is same with SC. It is found the  $m/n = 2/1$  mode are still survived after crash.

In this work, we have performed a totally nonlinear dynamics of the  $m/n = 1/1$  internal kink mode in EAST ohmic discharge and have reproduced SC with M3D. Based on the parameters and profiles of realistic EAST discharge plasma, our results show that  $m/n = 1/1$  kink mode is unstable, the rapid grows of unstable  $m/n = 1/1$  kink and interaction with its higher harmonics, are responsible for SC. Those results are consistent with theory [46]. The modeled SC has a complex crash phase, which consists more than two sub-crash oscillations. Our simulation uses a realistic resistivity values instead of a much larger one in other previous simulation work (with  $S = 1 \times 10^5$  or  $1 \times 10^6$ ). Furthermore, a  $m = 2$  island is found during the first-crash oscillation and the high mode number island, e.g.  $m = 4$  is formed after the second crash oscillation. These results are consistent with experimental observations of crash induced by 1/1 mode and  $m/n = 2/1$  island recovery after SLC. The rapid growing of  $m = 2$  tearing mode can lead to disruption also, however, M3D nonlinear simulations cannot find those crashes in our current work. This is not surprise, since the growth of  $m = 2$  resistive island is about two order slower than SC, and it is computationally prohibitive for the M3D code to reproduce  $m = 2$  islands developed crash with experimentally relevant resistivity values.

## 7. Summary and future work

In conclusion, a new upgraded SXR tomography system is used for SLC reconstruction in 2019 on EAST. A  $m/n = 2/1$  tearing mode dynamic related SLC has been investigated in detail. Nonlinear MHD simulation with M3D code has predicted the  $m/n = 1/1$  kink mode induced complex SC with realistic EAST parameters. Both the crashes of SLC and SC are due to nonlinear dynamics of  $m/n = 1/1$  instability. The  $m/n = 1/1$  instability in SLC is generated by toroidal and non-circular plasma shape effect of  $m/n = 2/1$  tearing mode. The role of 3D saturated  $m/n = 1/1$  kink mode in EAST improved H mode scenarios will be our future experiment plan. For numerical study, the simulation of the interaction and coupling of  $m/n = 1/1$  and  $m/n = 2/1$  are remain. Much longer simulations with experimental resistivity value or a much larger resistivity value to simulate of tearing mode-induced crash will be possible future work.

## Acknowledgments

This work was supported by the National Natural Science Foundation of China under Grant Nos. 11575247, 11975273 and 11605243. We would like to thank L. Sugiyama at MIT for providing M3D code. Liqing Xu would like to thanks Prof Liu Y at ASIPP for providing ECE data.

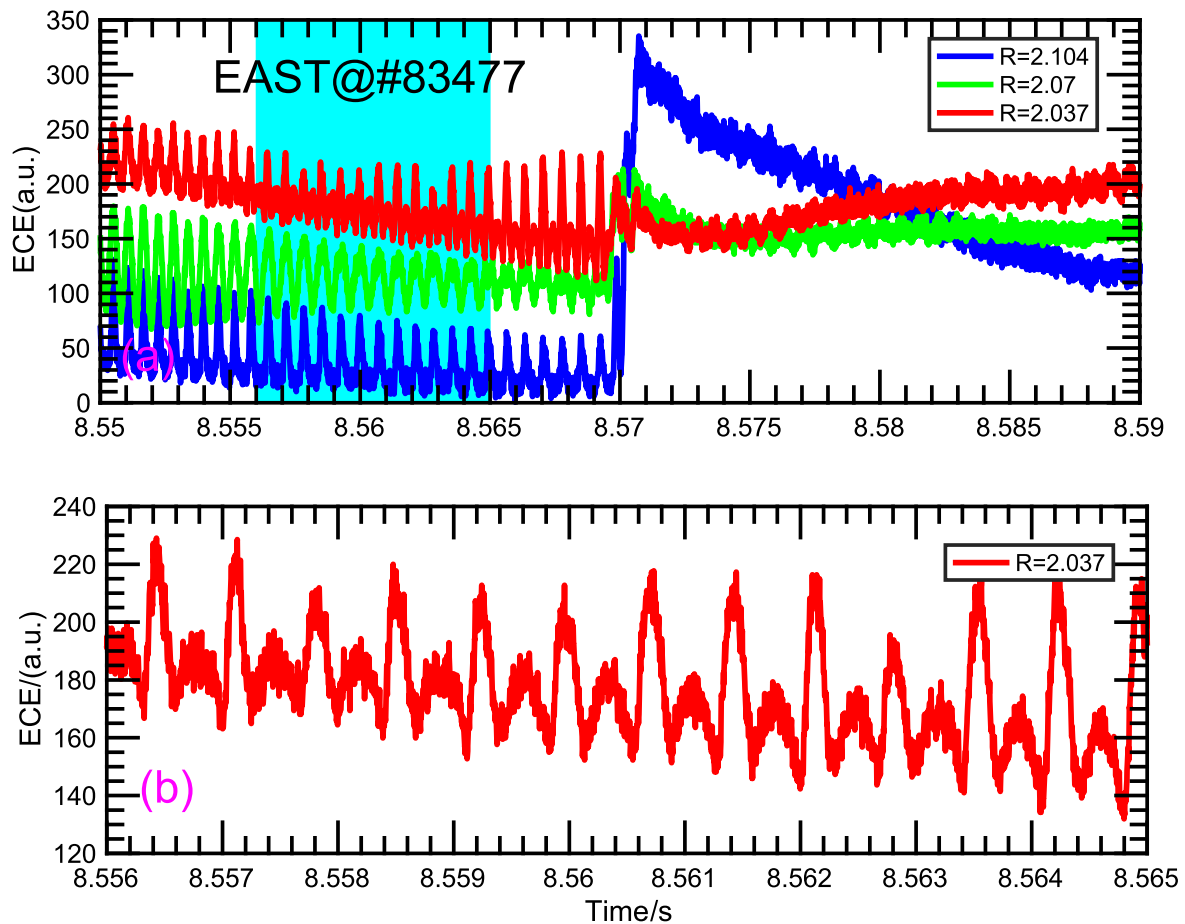


**Figure A1.** Identification of  $q = 2$  surfaces and  $m = 2$  island of  $m/n = 2/1$  tearing mode using ECE diagnostic. (a)—Three ECE channels measured  $m = 2$  instability; (b)—ECE channel with  $R = 2.037m$  inside  $m = 2$  island indicates the location of  $q = 2$  surface.

## Appendix.

### A1. Tearing mode identification

The location of  $q = 2$  surface plotted in the figure 4(h1) is determined by ECE diagnostic. The ECE measurements of  $m = 2$  mode also indicate the formation of  $m = 2$  island. As shown in figure A1(b), the formation of an additional peak in ECE channel means there is  $m = 2$  island [25]. Furthermore, the location of  $q = 2$  surface is marked by the channel inside of  $m = 2$  island ( $R_{q=2} \sim 2.037m$ ).

## References

- [1] von Goeler S, Stodiek W and Sauthoff N 1974 *Phys. Rev. Lett.* **33** 1201
- [2] Kadomtsev B 1975 *Sov. J. Plasma Phys.* **1** 389
- [3] Porcelli F, Boucher D and Rosenbluth M N 1996 *Plasma Phys. Control. Fusion* **38** 2163
- [4] Sun Y W, Wan B N, Hu L Q, Chen K Y, Shen B and Mao J S 2009 *Plasma Phys. Control. Fusion* **51** 065001
- [5] Igocine V, Dumbrajs O, Zohm H, Flaws A and ASDEX Upgrade team 2006 *Nucl. Fusion* **48** 062001
- [6] Breslau J, Jardin S and Park W 2007 *Phys. Plasma* **14** 056105
- [7] Sugiyama L 2014 *Phys. Plasma* **21** 022510
- [8] Sovinec C R, Gianakon T A, Held E D, Kruger S E, Schnack D D and NIMROD Team 2003 *Phys. Plasma* **10** 1727
- [9] Marx A and Lutjens H 2017 *Comput. Phys. Commun.* **212** 90
- [10] Shen W, Fu G Y, Sheng Z M, Breslau J A and Wang F 2014 *Phys. Plasma* **21** 092514
- [11] Nave M F F, Lazzaro E, Coelho R, Belo P, Borba D, Buttery R J, Nowak S, Serra F and EFDA-JET Contributors 2003 *Nucl. Fusion* **43** 179
- [12] Xu L Q et al 2017 *Nucl. Fusion* **57** 126002
- [13] Raj H et al 2018 *Nucl. Fusion* **58** 076004
- [14] Chapman I T, Scannell R, Cooper W A, Graves J P, Hastie R J, Naylor G and Zocco A 2010 *Phys. Rev. Lett.* **105** 255002
- [15] Hender T C et al 2016 *Nucl. Fusion* **56** 066002
- [16] Sertoli M, Dux R, Pütterich T and The ASDEX Upgrade Team 2015 *Plasma Phys. Control. Fusion* **57** 075004
- [17] Luce T C et al 2001 *Nucl. Fusion* **41** 1585
- [18] Joffrin E et al 2003 *Plasma Phys. Control. Fusion* **45** A367
- [19] Oyama N, Isayama A, Matsunaga G, Suzuki T, Takenaga H, Sakamoto Y, Nakano T, Kamada Y, Ide S and the JT-60 Team 2009 *Nucl. Fusion* **49** 065026
- [20] Petty C, Austin M E, Holcomb C T, Jayakumar R J, La Haye R J, Luce T C, Makowski M A, Politer P A and Wade M R 2009 *Phys. Rev. Lett.* **102** 045005
- [21] Wan B and EAST Team 2016 *Plasma Phys. Control. Fusion* **58** 014029
- [22] Chen K Y, Xu L Q, Hu L Q, Duan Y M, Li X Q, Yuan Y, Mao S T, Sheng X L and Zhao J L 2016 *Rev. Sci. Instrum.* **87** 063504



- [23] Liu Y, Schmuck S, Zhao H L, Fessey J, Trimble P, Liu X, Zhu Z Y, Zang Q and Hu L Q 2016 *Plasma Sci. Technol.* **18** 1148
- [24] Liu Y *et al* 2018 *Fusion Eng. Des.* **136** 72
- [25] Igochine V, Gude A, Gunter S, Lackner K, Yu Q, Barrera Orte L, Bogomolov A, Classen I, McDermott R M, Luhmann N C and ASDEX Upgrade Team 2014 *Phys. Plasma* **21** 110702
- [26] Gates D A, Delgado-Aparicio L and White R B 2013 *Nucl. Fusion* **53** 063008
- [27] Gates D A, Brennan D P, Delgado-Aparicio L, Teng Q and White R B 2016 *Phys. Plasmas* **23** 056113
- [28] Teng Q, Brennan D P, Delgado-Aparicio L, Gates D A, Swerdlow J and White R B 2016 *Nucl. Fusion* **56** 106001
- [29] Li G Q, Ren Q L, Qian J P, Lao L L, Ding S Y, Chen Y J, Liu Z X, Lu B and Zang Q 2013 *Plasma Phys. Control. Fusion* **55** 125008
- [30] Lopez-Bruna D, Ochando M A, Lopez-Fraguas A, Medina F and Asasibar E 2013 *Nucl. Fusion* **53** 073051
- [31] Tobias B *et al* 2016 *Phys. Plasma* **23** 056107
- [32] Furth H, Killeen J and Rosenbluth M N 1963 *Phys. Fluids* **6** 459
- [33] Nave M F F, Coelho R, Lazzaro E and Serra F 2000 *Eur. Phys. J. D* **8** 287
- [34] Fitzpatrick R 1994 *Phys. Plasma* **1** 3308
- [35] Suttrop W *et al* 1997 *Nucl. Fusion* **37** 119
- [36] La Hyaye R J, Brennan D P, Buttery R J and Gerhardt S P 2010 *Phys. Plasma* **17** 056110
- [37] Xu L Q, Hu L Q, Chen K Y, Li E Z, Zhang J Z, Zhou R J, Xu M and Chen Y B 2012 *J. Phys. Soc. Japan* **81** 064503
- [38] Edwards A W *et al* 1986 *Phys. Rev. Lett.* **57** 210
- [39] Buratti P, Giovannozzi E and Tudisco O 2003 *Plasma Phys. Control. Fusion* **45** L9–16
- [40] Chang Z *et al* 1996 *Phys. Rev. Lett.* **21** 3553
- [41] Sauter O *et al* 2002 *Phys. Rev. Lett.* **88** 105001
- [42] Xu L Q, Hu L Q, Chen K Y and Li M H 2014 *Chin. Phys. B* **23** 085201
- [43] Pfeiffer W, Marcus F B, Armentroutm C J, Jahns G J, Petrie T W and Stockdale R E 1985 *Nucl. Fusion* **25** 673
- [44] Janick C, Simm C, Decoste R, Pacher G W and Pacher H D 1990 *Nucl. Fusion* **30** 950
- [45] Campbell D J *et al* 1986 *Nucl. Fusion* **26** 1085
- [46] Aydemir A Y, Wiley J C and Ross D W 1989 *Phys. Fluids B* **1** 774